On the resolved scales in a turbulent boundary layer by tomographic PIV and PTV aided by VIC

Schneiders, Jan; Scarano, Fulvio; Elsinga, Gerrit

Publication date
2016

Document Version
Accepted author manuscript

Published in
Proceeedings of the 18th International Symposium on the Application of Laser and Imaging Techniques to Fluid Mechanics

Citation (APA)
Schneiders, J., Scarano, F., & Elsinga, G. (2016). On the resolved scales in a turbulent boundary layer by tomographic PIV and PTV aided by VIC. In *Proceeedings of the 18th International Symposium on the Application of Laser and Imaging Techniques to Fluid Mechanics: Lisbon, Portugal* Springer.

On the Resolved Scales in a Turbulent Boundary Layer by Tomographic PIV and PTV aided by VIC+

Jan F.G. Schneiders[1,*], Fulvio Scarano[1], Gerrit E. Elsinga[2]
1: Dept. of Aerospace Engineering, TU Delft, Delft, The Netherlands
2: Dept. of Mechanical, Maritime and Materials Engineering, TU Delft, Delft, The Netherlands
* Correspondent author: J.F.G.Schneiders@tudelft.nl

Keywords: Spatial Resolution, PIV/PTV processing, Turbulent Boundary Layer, Data Assimilation

ABSTRACT

Time-resolved tomographic PIV and tomographic PTV aided by VIC+ are applied in a turbulent boundary layer (Re_θ = 2038) measurement, and the resulting small scales flow properties, i.e. vorticity and dissipation, are compared. The VIC+ technique was recently proposed and uses the concept of *pouring time into space* to increase reconstruction quality of instantaneous velocity and vorticity. The tomographic PTV particle track measurements are interpolated to a dense grid, making use of both particle velocity and Lagrangian acceleration. The existing time-resolved tomographic PIV measurements by Jodai and Elsinga (2016, *J. Fluid Mech.* 795:611-633) are reprocessed using tomographic PTV and VIC+. Comparison of the vortical structures by visualization of isosurfaces of vorticity magnitude shows that the two methods return similar coherent vortical structures, but their strength in terms of vorticity magnitude is increased when using VIC+. Moreover, the results obtained by VIC+ provide additional detailing of the vortex shapes, which suggests an improvement in spatial resolution. Further statistical evaluation shows that the RMS of vorticity fluctuations from tomographic PIV are approximately 40% lower in comparison to a reference profile available from a DNS simulation, while the VIC+ technique returns RMS vorticity fluctuations to within 10% of the DNS reference. The dissipation rate is approximated by VIC+ to within approximately 10% for 25 < y+ < 120, in comparison to a damping of 50% by tomographic PIV. It is concluded that when time-resolved tomographic measurements are available, the VIC+ technique can improve reconstruction quality of velocity and vorticity – also in actual experiments.

1. Introduction

Following two decades of experimental and numerical work in wall-bounded turbulent flows, as reviewed in Marusic et al. (2010), todays experiments by tomographic PIV have allowed for unprecedented volumetric and time-resolved measurement of such flows (Schröder et al. 2008, 2011; Elsinga et al. 2010, 2012). Recent studies have however stumbled upon the spatial resolution limitations of tomographic PIV for measurements in a turbulent flow (Atkinson et al. 2011; Kähler et al. 2012; Lynch et al. 2014). Velocity fluctuations are typically dominated by large-scale events (i.e. the large scales contain most of the turbulent kinetic energy), and can be resolved well even with a relatively coarse spatial resolution. On the other hand, the vorticity and the other components of the velocity gradient, especially relevant for phenomena like turbulent kinetic energy dissipation are energetic at small scales and thus require higher spatial

resolution (typically a vector spacing of 2 Kolmogorov length scales, Tokgoz et al. 2012). This point is illustrated in figure 1 for a turbulent boundary layer. The velocity fluctuations measured by time-resolved tomographic PIV agree with DNS data within 5%, which is comparable to the uncertainty on the friction velocity used to represent the velocity in non-dimensional form. The rms vorticity profiles, instead, are systematically underestimated by approximately 40% when compared to the DNS. The spatial resolution in these measurements thus captures the velocity fluctuations accurately, but at the same time under-resolves the (peak) vorticity. For velocity statistics, subpixel accuracy and high spatial resolution can be achieved using a PTV (particle tracking velocimetry) approach in Kähler et al. (2012). For quantities requiring the evaluation of the instantaneous velocity gradient tensor (e.g. vorticity, strain rate, turbulent dissipation), the latter technique cannot be used and one needs to revert to the spatial resolution obtained from each snapshot.

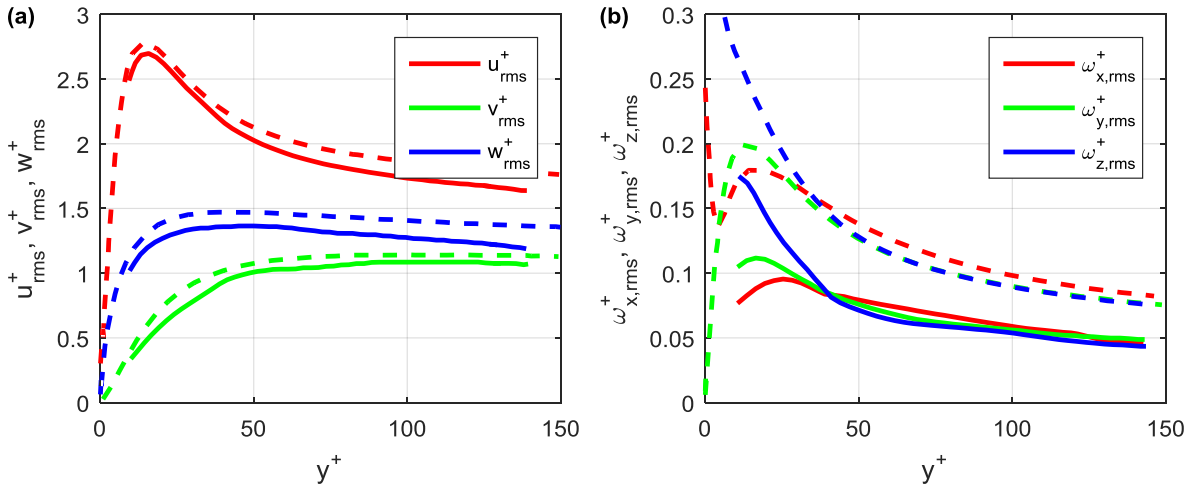

Fig. 1 Wall normal profiles of rms velocity (a) and vorticity (b), comparing the time-resolved tomographic PIV measurement of Jodai & Elsinga (2016) (solid lines) with the DNS database of Schlatter & Örlü (2010) (dashed lines). The x, y and z coordinates correspond to streamwise, wall-normal and spanwise directions, respectively.

The potential advantage of using a PTV approach to increase the dynamic range of instantaneous velocity and acceleration measurement fields from time-resolved Lagrangian particle tracking was explored by Novara et al. (2013). More elaborate algorithms are introducing data assimilation techniques to increase the velocity dynamic range and the spatial resolution for velocity measurements. The Shake-the-Box algorithm (Schanz et al. 2016) promises accurate Lagrangian particle tracking for densely seeded flows and was experimentally validated on the case of a circular jet flow in water. In cases where instead of spatial resolution, the temporal resolution is limited, the Vortex-in-Cell (VIC) technique has been successfully applied to tomographic PIV measurements to increase the temporal resolution (*Pouring Space*

into Time, Schneiders et al. 2014; Schneiders et al. 2016a). Recently this idea was reversed and the VIC technique was used to leverage temporal information from time-resolved tomographic PIV measurements for noise reduction in Schneiders et al. (2015a). Moreover, when dealing with time-resolved Lagrangian particle tracks (e.g. from tomographic PTV or 'Shake-the-Box'), the recently proposed VIC+ technique (Schneiders and Scarano 2016b) incorporates the temporal derivatives of velocity for instantaneous velocity reconstruction. The VIC+ technique was shown to increase spatial resolution when applied to a simulated experiment from a turbulent boundary layer. In particular, it was shown that the estimate of Reynolds stresses improved when using VIC+. Also, the work conducted within the European NIOPLEX consortium (Blinde et al. 2016) showed that the optimization produced with the VIC+ algorithm yields a very accurate reconstruction of the instantaneous pressure field, when compared to other methods based on cross-correlation analysis. It remains to be demonstrated whether similar improvements are achieved also in actual experiments, where factors such as image noise and calibration errors are present, leading to increased reconstruction noise and ghost particles (Elsinga et al. 2011).

The recent work from Jodai and Elsinga (2016) has adopted time-resolved tomographic PIV to obtain a detailed characterization of the turbulent motions in a turbulent boundary layer. The experiments showed good agreement with the reference DNS simulation (Schlatter & Örlü, 2010) in terms of velocity statistics (Figure 1a). However, the vorticity magnitude is systematically underestimated (Figure 1b), which is ascribed to the limited resolution of the measurement approach.

In the present work, the VIC+ technique is applied to the above measurements to assess the improvement in evaluating flow properties dominated by small-scale motions, such as vorticity and dissipation. The resulting enhancement in these quantities can subsequently be related to an increased spatial resolution of the whole measurement chain.

2. Experimental Setup

The time-resolved tomographic PIV turbulent boundary layer experiment in a water channel by Jodai and Elsinga (2016) is used in the present study. For full details of the experiment, the reader is referred to the latter manuscript. Salient details related to the boundary layer properties and measurement setup are recalled in this section. The free-stream velocity, U_∞, was 0.253 m/s with the free-stream turbulence intensity level of the water-tunnel below 0.7%. Further properties of the boundary layer are summarized in Tab. 1, where ν is the kinematic viscosity.

Tab. 1 Turbulent boundary layer properties.

U_∞	0.253 m/s
δ_{99}	69.9 mm
θ	7.70 mm
u_τ	0.0107 m/s
u_τ/ν	11.1 mm^{-1}
$Re_\tau = u_\tau \delta_{99}/\nu$	782
$Re_\theta = U_\infty \theta/\nu$	2038

Details of the tomographic measurement setup are listed in Tab. 2. The recording rate was chosen at 1279 Hz, resulting in approximately 3.3 pixels maximum particle displacement between frames, to allow for both analysis using PTV and PIV as outlined in Sec. 3. In total three time-series of 3140 images were recorded, corresponding to 7.37 s of observation time. For computational efficiency, in the present study not the full time-series is used for the analysis of the statistics. Results are taken at a time-separation of 0.6 s. Despite the small number of samples, the statistical evaluation of the turbulent flow properties is obtained considering the data ensemble along the homogeneous directions x and z. For further details of the experimental setup the reader is referred to Jodai and Elsinga (2016).

Tab. 2 Tomographic measurement setup.

Measurement volume	60 × 14.5 × 55 mm^3
Seeding	Hollow glass spheres (Sphericel)
	10 μm diameter
Illumination	Dual cavity 30 mJ/pulse Nd:YLF laser
Recording devices	4 × LaVision Imager Pro HS 4M
	2016 × 2016 pixels, 12-bit
Imaging	f = 105 mm Nikon objectives
Acquisition frequency	1279 Hz (single-frame mode)

3. Data Processing Methods

The measurement was originally processed using tomographic PIV as outlined in Sec. 3.1. As discussed above, the present manuscript proposes an alternative processing using VIC+ for increased reconstruction quality of the vorticity fluctuations. The VIC+ processing steps are outlined in Sec. 3.2. For both tomographic PIV and VIC+ processing, the same measurement data (i.e. recorded images) are used.

3.1 Tomographic PIV

Tomographic PIV processing was performed by Jodai and Elsinga (2016). Salient details related to the resolved length scales are recalled in this section. The intensity volumes were reconstructed using the MART algorithm (Elsinga et al. 2006) and the average intensity profile of the reconstruction in wall-normal direction as calculated from the reconstructed objects is re-plotted in Fig. 2a. The intensity shows a sharp increase at $y^+ = 0$, which marks the wall position. The illuminated region ranges up to $y^+ \approx 150$, after which the intensity decreases to the noise level.

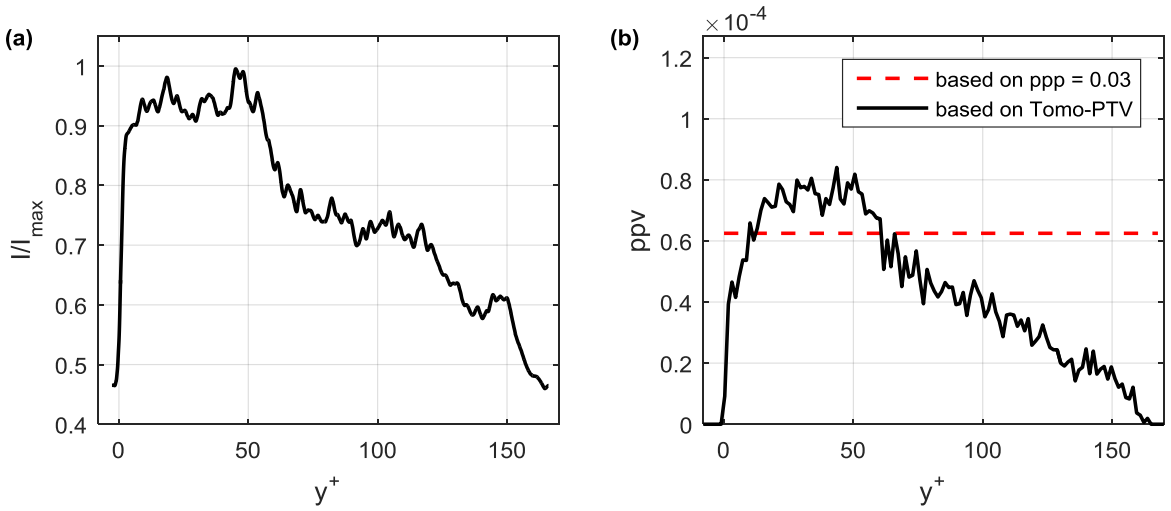

Fig. 2 Normalized profiles of reconstructed volume intensity (a) and identified particle track density (b) along wall-normal direction.

The particle displacement field was obtained from the sequence of reconstructed volumes using direct cross-correlation. For cross-correlation, the time-series was sub-sampled by a factor six, yielding a maximum particle displacement of 19 voxels, in order to enhance dynamic velocity range of the measurement. The first reconstructed volume was thus cross-correlated with the 7th volume in the time sequence, the 2nd with the 8th volume and so on. The resulting temporal oversampling of the velocity field was used later for filtering purposes. The final cross-correlation volume (interrogation volume) size was 32 × 32 × 32 voxels corresponding to 1.37 mm × 1.37 mm × 1.37 mm, with 75% overlap between neighboring interrogation volumes. The resulting vector spacing in each direction was 0.34 mm. The region close to the wall ($y^+ < 40$) was also processed using a final correlation window of 64 × 16 × 32 voxels at 75% overlap. This improves the spatial resolution in the wall-normal direction and accounts for the strong particle displacement gradient in that direction. The universal outlier detection method was used to remove spurious vectors (Westerweel and Scarano 2005). To suppress measurement noise, the velocity fields were spatiotemporally filtered using second-order polynomial regression over a period of 14.1 ms (1.7 wall units) and in a cubic filter volume of 2.05^3 mm^3, which corresponds to

23^3 wall-units. In the near-wall region, the filter volume was 4.10 mm × 1.02 mm × 2.05 mm (46 × 12 × 23 wall units) due to the different interrogation volume used. The coefficients of the polynomial regression were also used to determine the local velocity gradient.

3.2 Tomographic PTV with VIC+

To enable processing using VIC+, Lagrangian particle trajectories are evaluated using a tomographic PTV algorithm, which was used before by Schneiders et al. (2016c). The tomographic PTV algorithm uses the volumetric intensity distribution obtained with SMTE (Lynch and Scarano 2015) in LaVision Davis 8. Particle locations are identified with sub-voxel accuracy using a 3-point Gaussian fit along each coordinate direction. A particle-tracking algorithm based on Malik et al. (1993) is used to find particle tracks and the minimum acceleration criterion is used in case multiple tracks are identified within a search box. The tomographic PIV results (Sec. 3.1) are used as predictor for the tracking algorithm. The discrete positions of a particle in motion are then used to produce an estimate of the trajectory over 21 exposures using a 3rd order polynomial function, fitted through the particle locations. The result yields the fitted particle position at each time instant. Its time derivatives yield in turn the velocity and the Lagrangian acceleration (viz. velocity material derivative). Figure 2b shows the profile of identified particles per voxel (ppv) along wall-normal direction following from the PTV algorithm (black line). The water tunnel was seeded homogeneously and therefore a uniform track density is expected at an estimated level of ppv = 0.0006 (dashed red line), based on a ppp (particles per pixel) estimated to 0.03. In the region $10 < y^+ < 60$ slightly more particles are identified, which is ascribed to the enhanced particle detectability in this region due to the locally increased illumination intensity (Fig. 2a). It means that smaller particles (based on their scattering cross-sectional area) can be detected. For $y^+ < 10$ and $y^+ > 60$, instead, less tracks are identified than estimated from the ppp. This is ascribed to difficulty of tracking particles in the near-wall region and the region $y^+ > 60$ with lower laser light intensity, where particles can potentially disappear below the image noise level. No (ghost) particle trajectories are identified inside the wall region ($y^+ < 0$) or outside the measurement volume ($y^+ > 150$) by the tomographic PTV procedure.

After Lagrangian particle tracking, VIC+ yields a high-resolution interpolation of the scattered PTV measurements to a regular grid. The method works by finding the vorticity field that minimizes a cost function that includes both the PTV velocity and material derivative measurements and the result from VIC+. The quantities are related through the vorticity transport equation and the minimization problem is solved iteratively making use of the adjoint of the VIC code. The use of temporal information for reconstruction of instantaneous velocity is named *pouring time into space* and for further details of the method, the reader is referred to

Schneiders and Scarano (2016b). To start the iterative procedure, the tomographic PIV result is used as initial condition. The grid spacing is set to 0.25 mm, corresponding to 2.8 wall units and the no-slip condition is prescribed at the wall.

4. Results and discussion

The validity of the velocity reconstruction is first examined comparing it with the velocity statistics (Sec. 4.1). Subsequently, the instantaneous flow organization is studied (Sec. 4.2) and the statistics of vorticity fluctuations are considered (Sec. 4.3). The discussion concludes with the estimation of the dissipation rate (Sec. 4.4).

4.1 Velocity statistics

The velocity statistics are compared to the results by Schlatter & Örlü (2010) from a DNS simulation at Re_θ = 2000, which is close to the Reynolds number in the experiment (Re_θ = 2038). The performance of tomographic PIV using the cubic and elongated volumes for measurement of the velocity statistics in this experiment is already discussed in Jodai and Elsinga (2016). They are recalled here for comparison to the results from VIC+. The mean velocity profile along wall-normal direction is plotted in Fig. 3. The blue and yellow lines show the results obtained by tomographic PIV with respectively the cubic and elongated interrogation volumes. The red line shows the VIC+ result. For reference, the black line shows the DNS results. For 25 < y^+ < 140, all methods agree well with each other, indicating that the time averaged velocity profile is captured by all approaches and that the experiments agree with the DNS data.

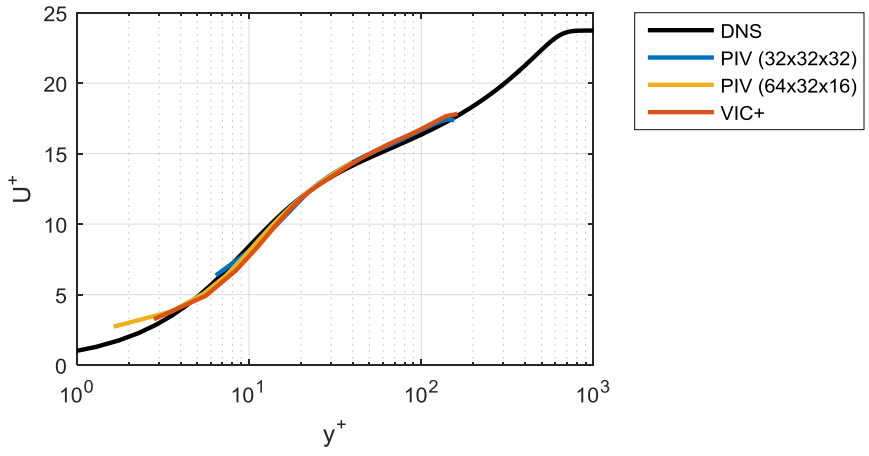

Fig. 3 Time-averaged velocity profiles returned by tomographic PIV with cubic and elongated correlation volumes and with VIC+, in comparison to the DNS result by Schlatter & Örlü (2010).

Closer to the wall (y^+ < 10), tomographic PIV with cubic interrogation volumes starts to deviate as it is unable to capture the strong particle displacement gradient in this region. With elongated correlation volumes the situation is improved, but still shows an overestimation for y^+ < 6 due to

interrogation windows overlapping with the wall below this wall-normal distance. With VIC+ the result for time-averaged streamwise velocity is similar to the PIV result with elongated volumes.

The profiles of rms velocity fluctuations are given in Fig. 4a-c, for respectively the streamwise, wall-normal and spanwise components of velocity. The PIV results with both cubic and elongated interrogation windows are largely equivalent, with the exception that the near wall peak at $y^+ = 15$ in the streamwise velocity fluctuations (Fig. 4a) is captured better by tomographic PIV with the elongated volumes. The VIC+ result of the streamwise velocity fluctuations (Fig. 4a) follows closely the PIV results, which match well with the DNS result for $y^+ < 50$ and return up to 10% reduced values for $y^+ > 50$. The reduced streamwise velocity fluctuations in this region are attributed to the slightly favorable pressure gradient in the facility and uncertainty in determining u_τ (Jodai and Elsinga 2016). For the wall-normal and spanwise velocity fluctuations (Fig. 4b and c, respectively), tomographic PIV shows again slightly lower values than the DNS result along the full profile, but remains within 10% between $y^+ = 50$ and 140. The VIC+ result, on the other hand, follows more closely the DNS result and remains within 3% for the wall-normal (Fig. 4b) and spanwise (Fig. 4c) components.

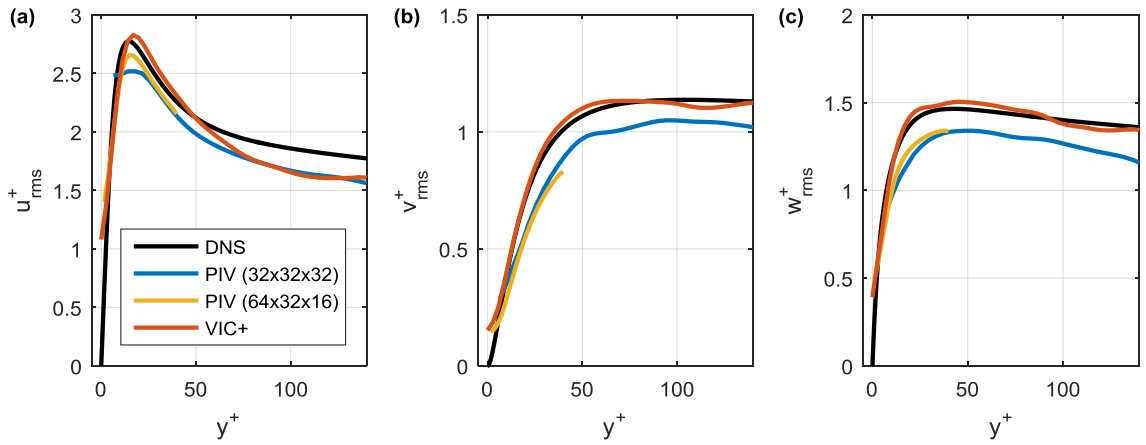

Fig. 4 Wall-normal profiles of rms velocity fluctuations returned by tomographic PIV with cubic and elongated correlation volumes and with VIC+, in comparison to the DNS result by Schlatter & Örlü (2010). Streamwise (a), wall-normal (b) and spanwise (c) velocity components.

Because divergence of velocity is expected to be zero in an incompressible flow, recent studies have used the level of velocity divergence to assess the measurement quality and accuracy of the velocity gradients (de Silva et al. 2013; Jodai and Elsinga 2016; amongst others). The velocity divergence consists of three components,

$$(1) \qquad \nabla \cdot \boldsymbol{u} = \frac{\partial u}{\partial x} + \frac{\partial v}{\partial y} + \frac{\partial w}{\partial z},$$

which in an incompressible flow add up to zero. The joint probability density function of $-\partial u/\partial x$ and $(\partial v/\partial y + \partial w/\partial z)$ is plotted in Fig. 5. Points away from the diagonal correspond to non-zero divergence. The comparison of the results obtained from tomographic PIV (a) and VIC+ (b) indicates a significantly lower divergence error for VIC+. The correlation coefficient of the two components plotted in Fig. 5 is 0.88 for the tomographic PIV result (Jodai and Elsinga 2016) and 0.9994 for VIC+. Additionally, the rms divergence error equals 0.013 wall units for PIV and 0.002 wall units for VIC+. This confirms that the VIC+ result is essentially divergence-free (i.e. satisfying the incompressibility constraint). Velocity divergence is not explicitly penalized during the VIC+ optimization procedure, but incompressibility is inherent to the method since it invokes the incompressible flow assumption.

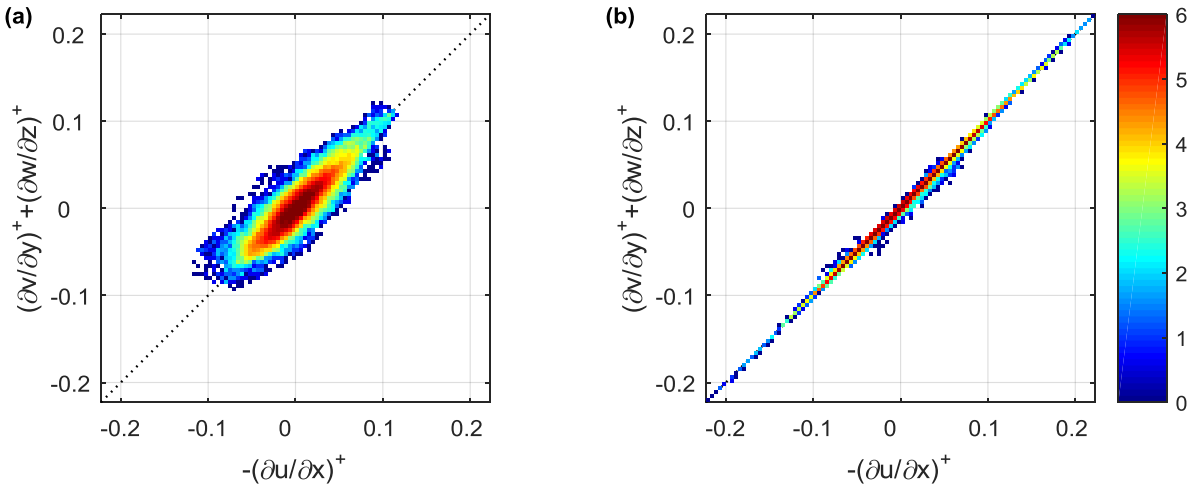

Fig. 5 Joint pdf of $-\partial u/\partial x$ and $(\partial v/\partial y + \partial w/\partial z)$ evaluated between y^+ = 40 and 60. The contours are plotted in log-scale. Tomographic PIV (a) and VIC+ (b).

4.2 Instantaneous flow organization

The flow organization in the measurement volume at a single time instant is given in Fig. 6, as reconstructed by tomographic PIV (a) and VIC+ (b). The figures illustrate the isosurfaces of vorticity magnitude ($|\boldsymbol{\omega}^+| = 0.3$, red, shaded by wall-normal distance for clarity) and streamwise velocity (blue, $\boldsymbol{u}^+ = 14$). From a qualitative inspection of the two data sets, a richer pattern of vortical structures is retrieved with the VIC+ reconstruction. For closer inspection, two hairpin vortices, S1 and S2, are indicated by arrows. The largest of the two, S1, is visible in both the tomographic PIV and VIC+ reconstructions. On the other hand, at the selected vorticity level, S2 is clearly visible only within the VIC+ reconstruction, where also two tongue-like appendices are revealed, attached to the hairpin structure.

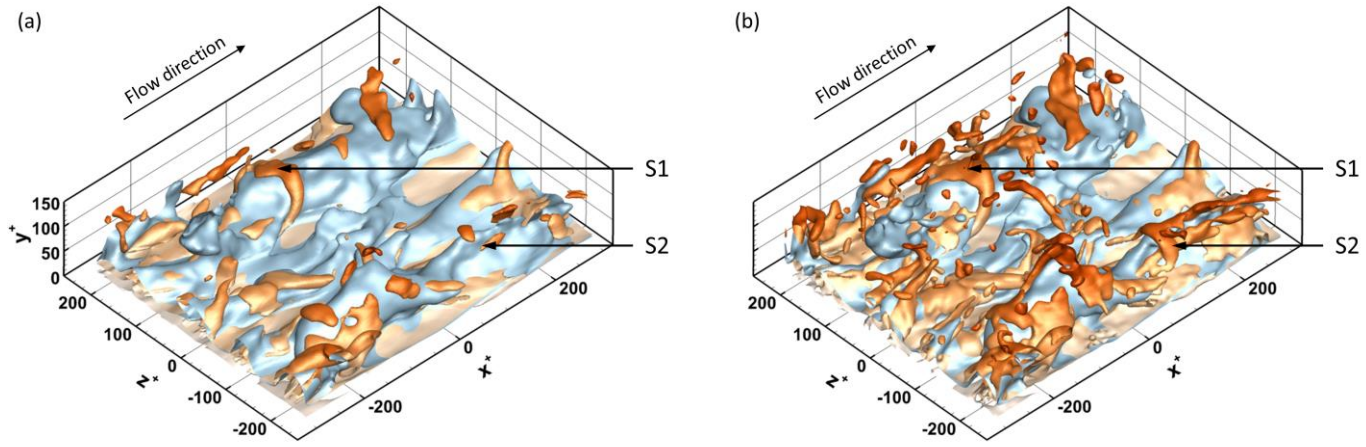

Fig. 6 Instantaneous flow organization in the measurement volume visualized by isosurfaces of vorticity magnitude ($|\boldsymbol{\omega}^+| = 0.3$, orange, shaded by wall-normal distance for clarity) and streamwise velocity ($\boldsymbol{u}^+ = 14$, blue). Tomographic PIV (a) and VIC+ (b).

For closer inspection, Fig. 7 shows a cut-out view of the hairpin structure S1, as reconstructed by tomographic PIV (a) and VIC+ (b). The in-plane velocity vectors are plotted in the plane x^+ = -35. Visual comparison shows no significant difference between the velocity vectors. Despite that streamwise vortex S3 is only marginally visible by the isosurface visualization in the PIV reconstruction, the velocity field does indicate the presence of the streamwise vortex. This indicates that the structure is present in both PIV and VIC+ results, but its associated vorticity magnitude is higher in the VIC+ result.

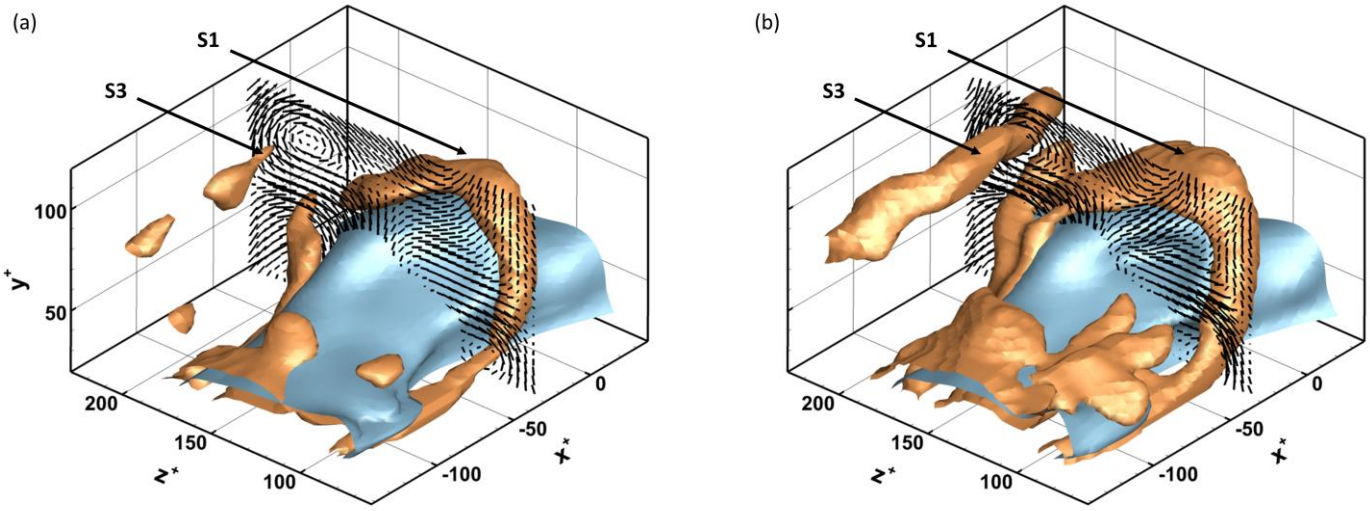

Fig. 7 Cut-out of hairpin structure S1, with the instantaneous in-plane velocity at x^+ = -35. The isosurfaces show vorticity magnitude ($|\boldsymbol{\omega}^+| = 0.35$, orange) and streamwise velocity ($\boldsymbol{u}^+ = 12$, blue). Tomographic PIV (a) and VIC+ (b).

The vorticity magnitude in the plane x^+ = -35 (corresponding to Fig. 7) is plotted in Fig. 8. The figure shows again the results from tomographic PIV (a) and VIC+ (b). The horizontal white line in the PIV result at y^+ = 35 indicates the border between the PIV results using cubic and elongated cross-correlation volumes. Furthermore, the vortical structures S1 and S3 are indicated by arrows. The figure confirms that both S1 and S3 are present in both results. The vorticity magnitude, however, differs by being higher in the VIC+ result.

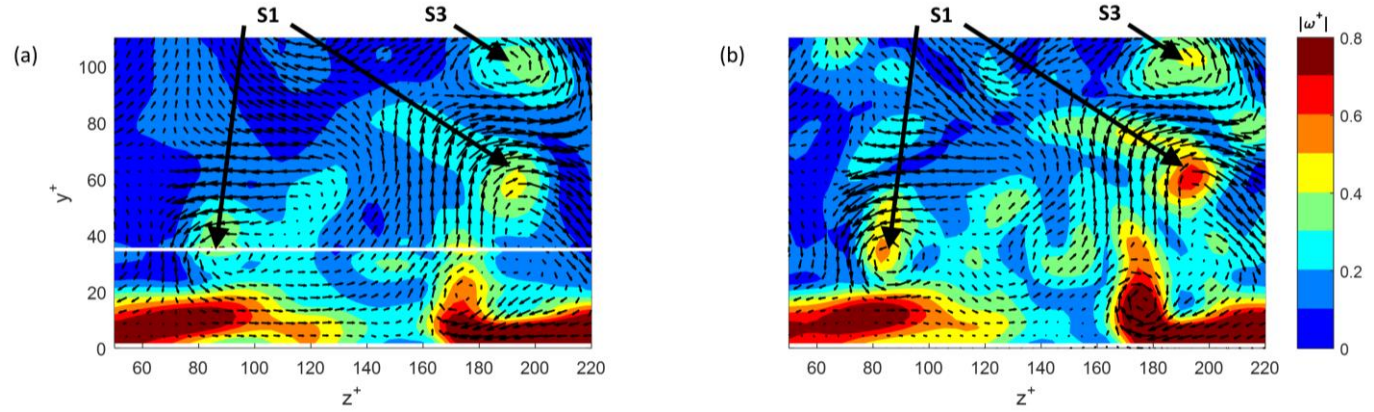

Fig. 8 Instantaneous field of vorticity magnitude at x^+ = -35 with velocity vectors (black) showing the in-plane velocity from tomographic PIV (a) and VIC+ (b). Velocity vectors are sub-sampled to a coarse mesh for clarity.

To investigate whether this is also the case for hairpin structure S2 (c.f. Fig. 6), a cut-out view of the hairpin vortex as calculated from tomographic PIV is given at three different isosurface levels of vorticity magnitude in Fig. 9a-c. Figure 9d shows the result by VIC+ at the highest isosurface level for PIV (Fig. 9c). At the decreased isosurface levels, the hairpin vortex and its tongues are visible from the PIV result in (a) and (b). Detail of the specific connection of the hairpin to the

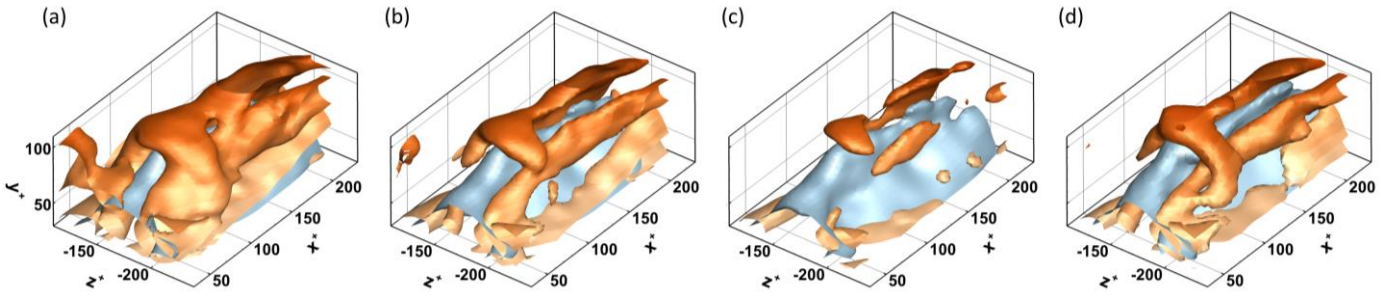

Fig. 9 Cut-out of hairpin structure S2. Isosurfaces of vorticity magnitude (orange) and streamwise velocity ($\boldsymbol{u}^+ = 14$, blue). Figures a-c show tomographic PIV with respectively isosurfaces of vorticity magnitude at $|\boldsymbol{\omega}^+|$ = 0.17, 0.23 and 0.3. Figure d shows the VIC+ result with $|\boldsymbol{\omega}^+|$ = 0.3.

tongues available from the VIC+ result (d), however, appears smeared out in the PIV result, indicating increased spatial resolution when VIC+ is employed. This suggests the effective spatial resolution is higher with VIC+ as compared to the tomographic PIV result.

4.3 Vorticity statistics

The analysis in the previous sections suggests that the VIC+ data evaluation returns increased vorticity magnitude within the vortices and therefore has the potential to restore the original amplitude of vorticity fluctuations. In this section the differences are quantified using the rms vorticity fluctuations, which are presented in Fig. 10. The blue and yellow lines show the results obtained by tomographic PIV with respectively cubic and elongated interrogation volumes. The red lines are for VIC+, while the black lines show the DNS result (Schlatter & Örlü 2010) for reference.

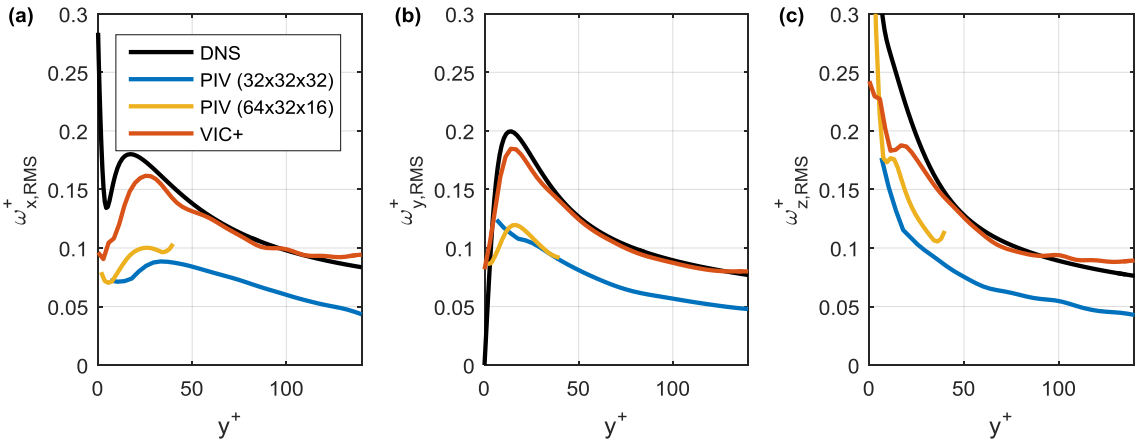

Fig. 10 Wall-normal profiles of rms vorticity returned by tomographic PIV with cubic and elongated correlation volumes and with VIC+, in comparison to the DNS result by Schlatter & Örlü (2010). Streamwise (a), wall-normal (b) and spanwise (c) rms vorticity fluctuations.

The rms streamwise vorticity fluctuations (Fig. 10a) by tomographic PIV are approximately 60% of the reference DNS level for $y^+ > 30$. In the near-wall region ($y^+ < 30$), a further reduction is observed with the cubic interrogation volumes, in comparison to the elongated volumes. For the wall-normal component (Fig. 10b), the tomographic PIV result with cubic interrogation volumes does not capture the peak rms vorticity level at $y^+ = 15$. The result with elongated interrogation volumes does capture the peak location, but gives an equal damping of the fluctuations to approximately 60% of the reference DNS level for $y^+ > 30$. A similar reduction in rms fluctuations for both cubic and elongated interrogation volumes is also obtained for the spanwise rms fluctuations (Fig. 10c). For comparison, a 35% reduction is expected with the present filter size used for tomographic PIV according to Saikrishnan et al. (2006), who assessed the effect of spatial filtering on the estimation of rms vorticity fluctuations. The reduced vorticity fluctuations

by tomographic PIV in the current experiment can therefore be largely ascribed to the effects of spatial filtering of the velocity field.

The red lines in Fig. 10 show the VIC+ result. For all three components of vorticity an increase in the level of rms fluctuations can be observed in comparison to tomographic PIV, which is consistent with the visualizations shown in Sect. 4.2. The streamwise vorticity fluctuations (Fig. 10a), are found within 10% of the reference from DNS for $y^+ > 20$. In the near-wall region ($y^+ < 20$), on the other hand, satisfactory agreement is not found even with the VIC+ method. Also for the spanwise vorticity fluctuations (Fig. 10c), in the near-wall region no satisfactory agreement is obtained and VIC+ yields a similar result as with tomographic PIV with elongated interrogation volumes. This is ascribed to the difficulty of obtaining reliable particle trajectories in the near-wall region. On the other hand, in the outer region ($y^+ > 20$), the VIC+ results for streamwise and spanwise vorticity fluctuations (Fig. 10a and c) agree to within 10% of the reference from DNS. The wall-normal vorticity fluctuations (Fig. 10b) reduce to zero at the wall, and are approximated within 10% from the DNS reference along the full profile. The data in Saikrishnan et al. (2006) shows that approximately 90% of the vorticity rms is captured at a spatial resolution of around 10 to 12 wall-units. Based on this, the effective spatial resolution of VIC+ in the present experiment is estimated at < 12 wall-units.

4.4 Dissipation rate

Compared to vorticity, the dissipation rate estimation is even more sensitive to spatial resolution, because it depends on velocity gradients raised to the power two. The underestimation of the dissipation rate by tomographic PIV is a problem recognized in recent literature (Tokgoz et al. 2012) and sub-grid scale modeling approaches have been proposed to improve estimation of approximation of the dissipation rate from PIV (Sheng et al. 2000; Bertens et al. 2015). Following the results in the previous section, an improved dissipation rate estimate in the range $20 < y+ < 140$ is expected with VIC+, in comparison to tomographic PIV. To assess this, the wall-normal profile of the turbulent kinetic energy dissipation rate is plotted in Fig. 11. The blue and yellow lines show the results obtained by tomographic PIV with respectively cubic and elongated interrogation volumes. The red line shows the VIC+ result. For comparison the DNS reference is plotted in black.

For the range $25 < y^+ < 140$ the tomographic PIV result underestimates the dissipation rate by ~50%. The VIC+ method yields a value within 10% at $25 < y^+ < 120$ with no need to introduce further sub-grid scale models. However, when considering the region close to the wall (Y<20) also the results of VIC+ appear to be affected by experimental errors that lead to an overestimation of the dissipation rate as for tomographic PIV.

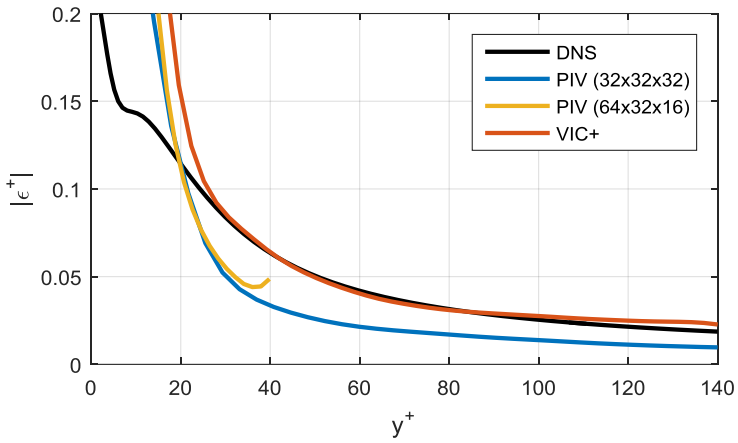

Fig. 11 Wall-normal profiles of kinetic energy dissipation rate returned by tomographic PIV with cubic and elongated correlation volumes and with VIC+, in comparison to the DNS result by Schlatter & Örlü (2010).

5. Conclusions

The VIC+ method is demonstrated to allow for measurement of rms vorticity fluctuations to within 10% of a reference from DNS, in a turbulent boundary layer at Re_θ = 2038 measured in a water tunnel. In comparison, tomographic PIV analysis yields approximately 40% damping of the vorticity fluctuations. Also, the dissipation rate is approximated by VIC+ to within approximately 10% of the DNS reference for 25 <y^+ < 120, in comparison to a damping of 50% by tomographic PIV. The effective spatial resolution of VIC+ in the present experiment is estimated at < 12 wall-units. Isosurface visualization of instantaneous velocity and vorticity shows increased coherence in the vortical structures at higher isosurface levels. The study demonstrates that the VIC+ method can be applied effectively to actual tomographic PIV measurements for increased reconstruction quality of velocity and vorticity.

Acknowledgements

This research is partly funded by LaVision GmbH.

References

Atkinson, C., Coudert, S., Foucaut, J. M., Stanislas, M., & Soria, J. (2011). The accuracy of tomographic particle image velocimetry for measurements of a turbulent boundary layer. Experiments in fluids, 50, 1031-1056.

Blinde P, Michaelis, D., van Oudheusden, B. W., Weiss, P.-E., de Kat, R., Laskari, A., Jeon, Y. J., David, L., Schanz, D., Huhn, F., Gesemann, S., Novara, M., McPhaden, C., Neeteson, N., Rival, D., Schneiders, J. F. G., Schrijer, F. (2016) Comparative assessment of PIV-based pressure evaluation techniques applied to a transonic base

flow. In: 18th international symposium on the application of laser techniques to fluid mechanics. Lisbon, Portugal. 4-7 July.

Bertents, G., van der Voort, D., Bocenagra-Evans, H., & van de Water, W., (2015) Large-eddy estimate of the turbulent dissipation rate using PIV. Experiments in Fluids. 56, 89.

De Silva, M. C., Philip, J., Marusic, I. (2013) Minimization of divergence error in volumetric velocity measurements and implications for turbulence statistics. Experiments in Fluids. 54, 1557.

Elsinga, G. E., Scarano, F., Wieneke, B., & van Oudheusden, B. W. (2006). Tomographic particle image velocimetry. Experiments in fluids, 41, 933-947.

Elsinga, G. E., & Marusic, I. (2010). Evolution and lifetimes of flow topology in a turbulent boundary layer. Physics of Fluids, 22, 015102.

Elsinga, G. E., & Westerweel, J., Scarano, F., & Novara, M. (2011). On the velocity of ghost particles and the bias errors in Tomographic-PIV. Experiments in fluids, 50, 825-838.

Elsinga, G. E., Poelma, C., & Schröder, A., Geisler, R., Scarano, F., & Westerweel, J. (2012). Tracking of vortices in a turbulent boundary layer. Journal of Fluid Mechanics, 697, 273-295.

Jodai, Y., & Elsinga, G.E. (2016) Experimental observation of hairpin auto-generation events in a turbulent boundary layer. Journal of Fluid Mechanics. 795:611-633.

Kähler, C. J., Scharnowski, S., & Cierpka, C. (2012). On the uncertainty of digital PIV and PTV near walls. Experiments in fluids, 52, 1641-1656.

Lynch, K., Pröbsting, S., & Scarano, F. (2014). Temporal resolution of time-resolved tomographic PIV in turbulent boundary layers. In: 17th international symposium on the application of laser techniques to fluid mechanics. Lisbon, Portugal.

Malik, N. A., Dracos, T., & Papantoniou, D. A. (1993). Particle tracking velocimetry in three-dimensional flows. Experiments in Fluids, 15, 279-294.

Marusic, I., McKeon, B. J., Monkewitz, P.A., Nagib, H.M., Smits, A.J., & Sreenivasan, K.R. (2010) Wall-bounded turbulent flows at high Reynolds numbers: Recent advances and key issues. Phys. Fluids 22, 065103, 1-24.

Novara, M., & Scarano, F. (2013). A particle-tracking approach for accurate material derivative measurements with tomographic PIV. Experiments in fluids, 54, 1-12.

Saikrishnan, N., Marusic, I., Longmire, E.K. (2006) Assessment of dual plane PIV measurements in wall turbulence using DNS data. Experiments in fluids, 41, 265–278

Schanz, D., Gesemann, S., & Schröder, A. (2016). Shake-The-Box: Lagrangian particle tracking at high particle image densities. Experiments in fluids, 57, 70.

Schlatter, P. & Örlü, R. 2010 Assessment of direct numerical simulation data of turbulent boundary layers. J. Fluid Mech. 659, 116-126.

Schneiders, J. F. G., Dwight, R. P., & Scarano, F. (2014). Time-supersampling of 3D-PIV measurements with vortex-in-cell simulation. Experiments in Fluids, 55, 1692.

Schneiders, J. F. G., Dwight, R. P., & Scarano, F., (2015a) Tomographic PIV noise reduction by simulating repeated measurements. In: 11th International Symposium on Particle Image Velocimetry, PIV15, Santa Barbara, CA, USA, September 14-16.

Schneiders, J. F. G., Pröbsting, S., Dwight, R. P., van Oudheusden, B.W., & Scarano, F. (2016a). Pressure estimation from single-snapshot tomographic PIV in a turbulent boundary layer. Experiments in Fluids, 57, 53.

Schneiders, J. F. G., Scarano, F. (2016b). Dense Velocity Reconstruction from Tomographic PTV with Material Derivatives. *Under Review*

Schneiders, J. F. G., Caridi, G. C. A., Sciacchitano, A., & Fulvio Scarano. (2016c) Instantaneous Pressure Measurements from Large-Scale Tomo-PTV with HFSB Tracers past a Surface-Mounted Finite Cylinder. In: 54th AIAA Aerospace Sciences Meeting. San Diego, CA, USA, January 4-8.

Schröder, A., Geisler, R., Elsinga, G. E., Scarano, F., & Dierksheide, U. (2008). Investigation of a turbulent spot and a tripped turbulent boundary layer flow using time-resolved tomographic PIV. Experiments in Fluids, 44, 305-316.

Schröder, A., Geisler, R., Staack, K., Elsinga, G. E., Scarano, F., Wieneke, B., Henning, A., Poelma, C., & Westerweel, J. (2011). Eulerian and Lagrangian views of a turbulent boundary layer flow using time-resolved tomographic PIV. Experiments in Fluids, 44, 305-316.

Sheng, J., Meng, H., & Fox, R. (2000) A large eddy PIV method for turbulence dissipation rate estimation. Chem. Eng. Sci. 55, 4423–4434

Tokgoz, S., Elsinga, G. E., Delfos, R., & Westerweel, J. (2012). Spatial resolution and dissipation rate estimation in Taylor--Couette flow for tomographic PIV. Experiments in fluids, 53, 561-583.

Westerweel, J., & Scarano, F. (2005) Universal outlier detection for PIV data. Experiments in fluids, 39, 1096–1100.